ACS central science

Research Article

http://pubs.acs.org/journal/acscii

Core–Shell Nanoparticle Coating as an Interfacial Layer for Dendrite-Free Lithium Metal Anodes

Wei Liu,[†] Weiyang Li,[†] Denys Zhuo,[†] Guangyuan Zheng,[†] Zhenda Lu,[†] Kai Liu,[†] and Yi Cui*[,†,‡]

[†]Department of Materials Science and Engineering, Stanford University, Stanford, California 94305, United States

[‡]Stanford Institute for Materials and Energy Sciences, SLAC National Accelerator Laboratory, 2575 Sand Hill Road, Menlo Park, California 94025, United States

Supporting Information

ABSTRACT: Lithium metal based batteries represent a major challenge and opportunity in enabling a variety of devices requiring high-energy-density storage. However, dendritic lithium growth has limited the practical application of lithium metal anodes. Here we report a nanoporous, flexible and electrochemically stable coating of silica@poly(methyl methacrylate) (SiO_2@PMMA) core–shell nanospheres as an interfacial layer on lithium metal anode. This interfacial layer is capable of inhibiting Li dendrite growth while sustaining ionic flux through it, which is attributed to the nanoscaled pores formed among the nanospheres. Enhanced Coulombic efficiencies during lithium charge/discharge cycles have been achieved at various current densities and areal capacities.

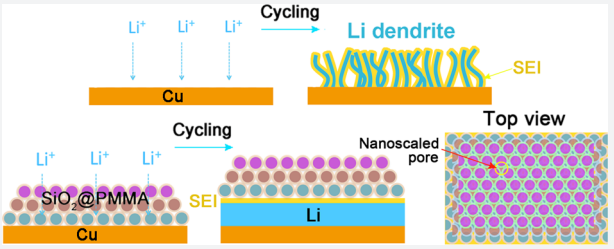

Considerable effort has been devoted to improving current rechargeable lithium batteries, owing to the ever-increasing demand for high-energy-density, safe and economical energy storage for portable electronics as well as electric vehicles.[1,2] Lithium metal is the most attractive anode candidate as a result of its high theoretical specific capacity of 3860 mAh g^{-1} (compared to 372 mAh g^{-1} for carbon anode) and its low electrochemical potential (−3.04 V versus standard hydrogen electrode). Lithium metal therefore is the choice of anode for advanced high-energy batteries such as Li–S battery, Li–air battery, and the like.[3−5] However, the formation and growth of Li dendrites during repeated cycles of charge/discharge and the highly reactive nature of Li metal limit the commercialization of lithium metal anode.

Different graphite and silicon anodes undergo volume changes of about 10% and 400% respectively during the lithiation process; Li metal is a "hostless" electrode with a virtually infinite relative volume change during Li stripping/plating leading to significant mechanical instability. In addition, the highly reactive Li metal can decompose the liquid electrolyte to form an insoluble layer of solid–electrolyte interphase (SEI). This unstable SEI layer cannot accommodate the unavoidable volume change, which introduces the formation of cracks, pits, and crevices with low impedance during Li plating/striping. Subsequently, the cracks in the SEI expose fresh Li metal and locally enhance the flux of lithium ions, which in turn further promotes the growth of uneven Li filaments and dendrites. Furthermore, dendritic Li with large specific surface area can continuously decompose the electrolyte, resulting in low Coulombic efficiency and short cycle life (Figure 1a).[6−10] These dendrites can ultimately occupy all of the free space in the battery and penetrate the separator, leading to a short circuit in the cell, and cause overheating and fire.

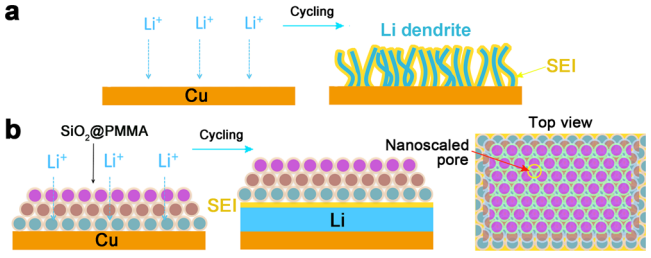

Figure 1. Schematic diagrams of the different Li anode structures. (a) A thin film of SEI layer forms quickly on the bare Cu surface of deposited Li. Volumetric changes during the Li deposition process can easily break the SEI layer, especially at high current rates. This behavior leads to ramified growth of Li dendrites and rapid consumption of the electrolyte. (b) Modified Cu electrode coated with a SiO_2@PMMA nanosphere layer. The volumetric change of Li deposition/dissolution is accommodated by the coating of SiO_2@PMMA nanospheres. Nanoscaled pores are able to suppress lithium dendrites. Note that in order to indicate the packing of nanospheres more clearly, each monolayer is given a different color.

Accordingly, a large number of studies have explored various approaches to suppress lithium dendrites by improving the stability and uniformity of the SEI on the lithium anode surface by optimization of solvents,[11] salts,[12,13] electrolyte additives,[14,15] and inorganic compounds.[16] The formation of alloys during Li deposition using metal cation additives has also been considered.[17−20] Although these approaches are promising, the

Received: December 15, 2016
Published: February 8, 2017

DOI: 10.1021/acscentsci.6b00389
ACS Cent. Sci. 2017, 3, 135−140

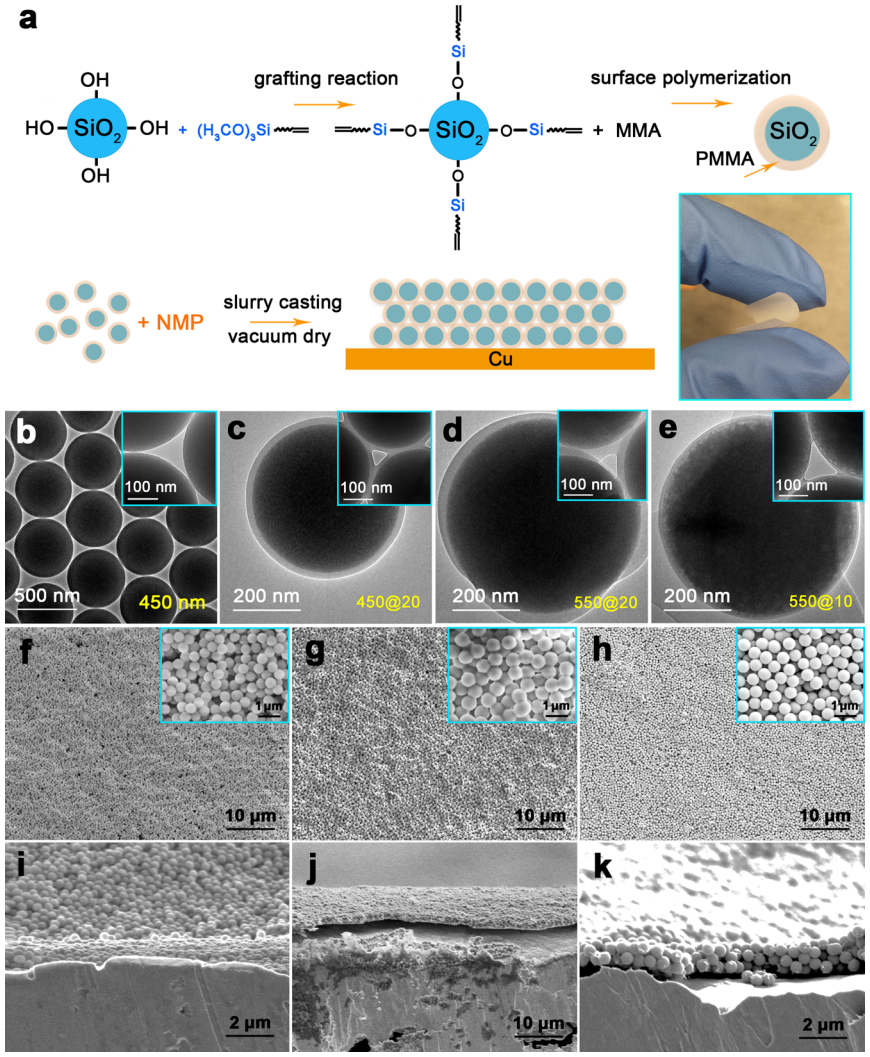

Figure 2. Schematic diagrams for the preparation of SiO_2@PMMA core−shell nanosphere coated electrode and microstructures for nanospheres with various dimensions. (a) SiO_2 nanospheres were first functionalized with $(H_3CO)_3Si$. Monodisperse SiO_2@PMMA core−shell nanospheres were synthesized by seeded emulsion polymerization. SiO_2@PMMA nanosphere coated Cu electrodes were synthesized by slurry casting. The inset figure indicates that the membrane (thickness is 5 μm) formed by the SiO_2@PMMA core−shell nanospheres is flexible. (b) TEM image of the SiO_2 nanospheres. (c−e) TEM images of the SiO_2@PMMA nanospheres of (c) 450@20, (d) 550@20, and (e) 550@10 nm. The inset figures show the subtriangular pores formed between three nanospheres with various diameters. (f−k) Top-view and cross-sectional SEM images of the SiO_2@PMMA nanospheres with (f, i) 450@20, (g, j) 550@20, and (h, k) 550@10 nm coated on Cu foil.

performance is still not satisfactory as the weak SEI film cannot completely eliminate dendrite growth[21] and consumption of the additives to depletion. Therefore, various rational designs of a "host" for lithium have been demonstrated including hollow carbon spheres,[22] graphene oxides,[23] and carbon[24] and polymer nanofibers.[25] Moreover, various interfacial layers have been also proposed to impede the Li dendrite growth,[26−28] including hollow carbon spheres,[26] boron nitride,[27] and graphene.[28] Solid state electrolyte can block Li dendrite growth although most of them have limited ionic conductivity and low interfacial chemical stability.[29−31]

Building a robust interface layer capable of accommodating the volumetric expansion of Li deposition without breaking yet suppressing dendrite growth without blocking Li-ion conduction would be a promising approach. Herein, we demonstrate a nanoporous, flexible and electrochemically stable coating of SiO_2@PMMA core−shell nanospheres on lithium metal anode which successfully addresses the previously outlined concerns. Lithium dendrites are likely to be blocked by the coating of SiO_2@PMMA core−shell nanospheres, due to the high modulus of 68 GPa for the SiO_2 core.[32] It should be noted that the elastic modulus of the layer of SiO_2@PMMA core−shell nanospheres would give a better metric for whether it is theoretically prone to resist lithium dendrite growth. The PMMA shell serves to adhere the SiO_2 nanospheres together to form a robust and flexible membrane which also protects the SiO_2 from reacting with Li. The nanoscaled pores formed among the packed core−shell nanospheres are small enough, which would be smaller than critical nucleation size of Li metal dendrite (several hundred nanometers),[27] which does not allow thin dendrite to penetrate through, as illustrated in Figure 1b. When there is SEI formed on Li metal, the bottom of such a nanoporous film can be part of the SEI composite.

Morphological and Structural Analysis. SiO_2 nanospheres with various diameters were synthesized by a modified Stöber synthesis according to the literature.[33] Figure 2b displays the transmission electron microscope (TEM) image for the spherical SiO_2 particles with a close-packed aggregate, showing

DOI: 10.1021/acscentsci.6b00389
ACS Cent. Sci. 2017, 3, 135−140

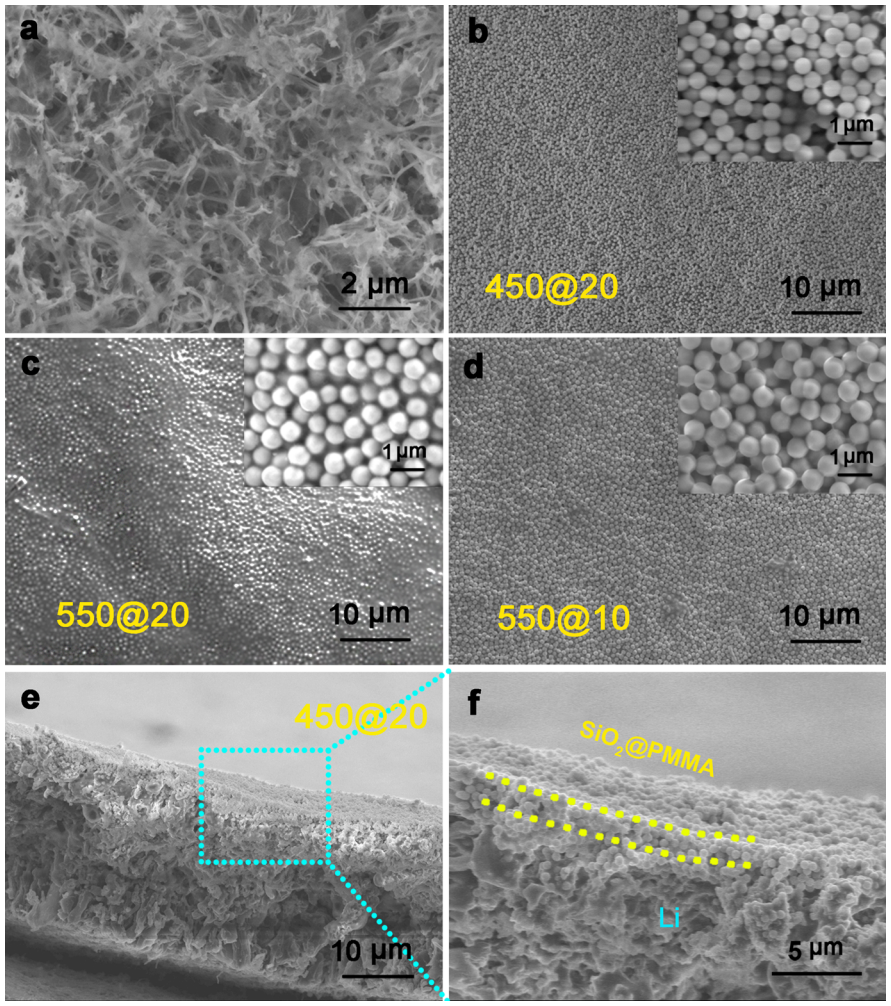

Figure 3. Li deposition on Cu substrate with and without protective layer of SiO_2@PMMA nanospheres. (a) Top-view SEM image of deposited Li metal on bare Cu substrate. (b–d) Top-view SEM images of the 10th lithium deposition on Cu substrate with interfacial layer of SiO_2@PMMA nanosphere of (b) 450@20, (c) 550@20, and (d) 550@10 nm at current rate of 1.0 mA cm^{-2}. (e, f) Cross-sectional SEM images of the 10th lithium deposition on Cu substrate with interfacial layer of SiO_2@PMMA nanospheres of 450@20 nm.

a uniform distribution of diameters. Three SiO_2 nanopheres adjoin together to form a pore that shows an approximate triangular shape (here we only consider two-dimensional packing plane) with nanometer scale length. Monodisperse and concentric SiO_2@PMMA core–shell nanocomposites were synthesized by seeded emulsion polymerization,[34] as schematically illustrated in Figure 2a. In a typical synthesis, silica colloids modified by 3-(trimethoxysilyl)propyl methacrylate (MPS), sodium dodecyl sulfate, methyl methacrylate (MMA), water, and isopropanol were mixed in a three-necked round-bottomed flask. After degassing with nitrogen, the mixture was heated to 70 °C, followed by an injection of potassium persulfate (KPS) solution to initiate the polymerization. The reaction was maintained at 70 °C for 7 h. The concentration of MMA can be controlled to modify the thickness of the PMMA shell. It is found that the thickness of the PMMA shell increases uniformly with the concentration of MMA monomers at the early stage of polymerization, forming concentric core–shell nanosphere morphology. With continuous polymerization, excess MMA monomers are absorbed in the cross-linked polymer networks, which results in phase separation of the monomer from the network and eventually additional bulges attaching to the original particles and even free PMMA colloids, due to the elastic stress driven by the entropy change of the swollen networks. Therefore, higher concentration of MMA monomers increases the possibility of phase separation, ellipsoidal bulges, and free colloids.[34] However, careful multiple centrifugations are able to remove the free PMMA nanoparticles. The monodisperse core–shell nanospheres were then dispersed in *N*-methylpyrrolidone (NMP) with the aid of ultrasonic agitation. Finally, the coating of SiO_2@PMMA core–shell nanospheres on Cu foil was easily obtained by casting with a doctor blade and then dried in vacuum overnight to completely remove the NMP solvent. It can be seen that the freestanding membrane (thickness is 5 μm) formed by the SiO_2@PMMA core–shell nanospheres is highly flexible, as shown in the inset photo of Figure 2a.

Fourier transform infrared (FTIR) transmittance spectra in Figure S1 confirm that PMMA is successfully coated on the surface of SiO_2 by the appearance of C═O bond for the nanospheres after polymerization.[35] Thermogravimetry (TG) is widely used for the determination of the weight ratio of inorganic/organic hybrid composites. As shown in Figure S2, the TG curves show that a rapid weight loss around 350–400 °C is mainly due to the dehydrogenation of PMMA. After the decomposition of PMMA, the inorganic SiO_2 core remains,

DOI: 10.1021/acscentsci.6b00389
ACS Cent. Sci. 2017, 3, 135–140

showing a weight ratio of about 70% and 55% for 550@10 and 550@20 nm (defined as diameter of the silica core @ thickness of the PMMA shell) nanopheres, respectively.

A series of TEM images (Figure 2c–e and Figure S3) show the morphologies of SiO_2@PMMA core–shell nanopheres, which indicate that the SiO_2 nanoparticle lies in the center of the colloids with clearly distinguishable core–shell structures. The SiO_2 cores with diameters of 350, 450, and 550 nm and the PMMA shells with thicknesses ranging from 10 to 45 nm were synthesized controllably. Figure 2f–h shows the top view SEM images of the coatings consisting of SiO_2@PMMA nanospheres, indicating a uniform morphology with high porosity. The cross-sectional SEM images (Figure 2j,k) exhibit that the neat and flat coatings consist of approximately three monolayers of SiO_2@PMMA nanospheres with around 1.2 μm thickness. The digital photos and optical images in Figure S4 show the Cu foils coated with nanospheres layers after sticking and stripping from tapes (colored label tape, Fisher Scientific), suggesting a strong adhesion between Cu foil and coating layer. The SiO_2@PMMA coating is capable of accommodating the bending of the Cu foil without the appearance of cracks, as shown in Figure S4d–g.

For an interfacial porous layer with the function of blocking lithium dendrite and sustaining the ionic flux through it, the pore structure directly determines its permeability, tortuosity, and ionic conductivity and then affects battery performance. For the same thickness of coating, it should be noted that smaller pores might give rise to a longer pathway due to the increased tortuosity, compared with larger pores that are able to provide a more direct pathway and higher ionic conductivity. Increasing the pore size can also reduce the membrane's mechanical properties. Therefore, the pore size of the interfacial porous layer plays a significant role in determining the electrochemical performance of lithium metal anode due to the trade-off between ionic conductivity and modulus.[36,37] It can be seen from the inset images in Figure 2c–e that the size of the subtriangular pore increases with the increase in diameter of SiO_2 and decrease in thickness of PMMA. Typically, for 550@10 nm SiO_2@PMMA nanospheres, the length of the triangular pore is about 120 nm, which is small enough to prevent Li dendrite growth (critical size is several hundred nanometers) but large enough that it does not hinder the transport of Li ions.[27] The electrochemical performance of the cell using the electrode coated with SiO_2@PMMA nanospheres may be improved based on this special microstructure.

Electrochemical Testing. Investigation of dendrite growth was carried out under conditions of Li plating/stripping at a current rate of 1 mA cm^{-2} and deposition capacity of 2 mAh cm^{-2} after 10 cycles, as shown in Figure 3. The direct deposition of Li metal onto a bare Cu electrode results in ragged growth of mossy Li dendrites (Figure 3a). In sharp contrast, Li dendrites do not appear on the electrode coated with an interfacial layer of SiO_2@PMMA nanospheres (Figure 3b–d). Instead, an evenly confined deposition of Li underneath the coating is observed (Figures 3e and 3f). Compared with SiO_2@PMMA nanospheres before the deposition/dissolution of lithium, the coating after multiple cycles shows little variation in the morphologies, which indicates the good physical stability of the coatings. Therefore, the modulus of the layer of SiO_2@PMMA core–shell nanospheres is high enough to block lithium dendrite growth. The SiO_2@PMMA nanosphere layer is capable of suppressing dendritic lithium by acting as a robust and conformal shield.

To substantiate the practicality of a SiO_2@PMMA nanosphere modified electrode and its chemical stability in contact with lithium metal, a coin cell consisting of this electrode and lithium foil as counter electrode were used to study the cycling stability and Coulombic efficiency of Li plating/stripping, as shown in Figures 4a and 4b. 1 M LiPF6 in 1:1 ethylene

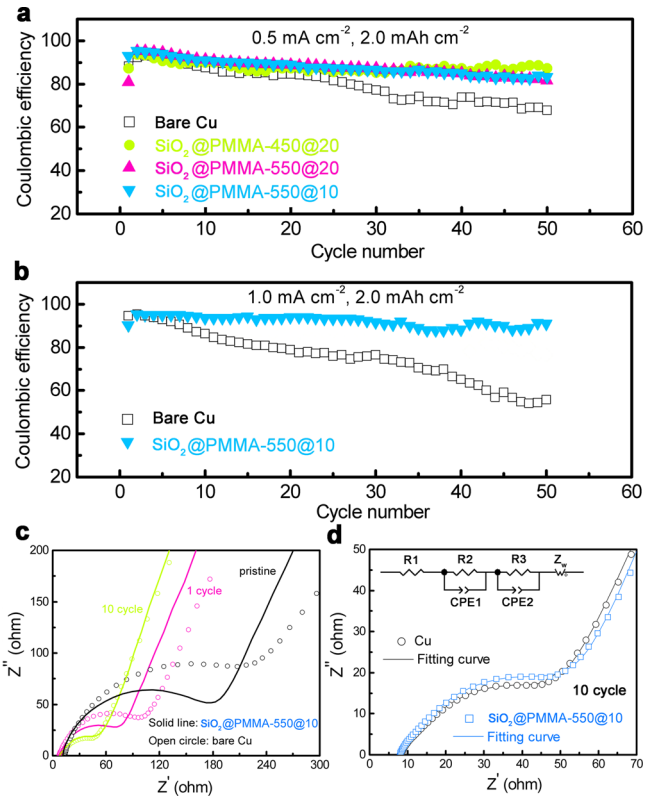

Figure 4. Electrochemical characterization of the electrodes for Li deposition/dissolution. (a, b) Comparison of Coulombic efficiency of Li metal anode with and without SiO_2@PMMA nanosphere coating at various current rates of (a) 0.5 mA cm^{-2} and (b) 1.0 mA cm^{-2} with the same areal capacity of 2.0 mAh cm^{-2}. (c) Experimental impedance spectra for the electrode with and without interfacial layer of SiO_2@PMMA nanospheres before and after the first and 10th cycles. (d) Experimental and fitted impedance spectra for the electrode with and without coating after the 10th cycle, and equivalent circuit. In the equivalent circuit, R1 is the electrolyte resistance. R2 and R3 correspond to the current collector/electrolyte interface and Li/electrolyte interface, respectively. CPE1 and CPE2 are the constant phase elements to fit capacitances. The straight line in the lower frequencies is due to an ion diffusion limited process contributing to an impedance response (Warburg impedance Z_w).

carbonate (EC) and diethyl carbonate (DEC) (BASF Selectilyte LP40) was added as electrolyte. The Coulombic efficiency of the Li deposition/dissolution can be calculated from the capacity ratio of Li removed from the Cu electrode to that deposited during the same cycle. The cell with bare Cu electrode shows a gradual decrease in Coulombic efficiency, which eventually decays to 68% and 56% after 50 cycles at 0.5 mA cm^{-2} and 1.0 mA cm^{-2}, respectively. It is reasonable that less and less Li can be stripped from the Cu electrode with each cycle of deposition/dissolution since a large surface area of Li metal dendrites consumes electrolyte very fast. For the Cu electrode coated with SiO_2@PMMA nanospheres of 450@20, 550@10, and 550@20 nm, the Coulombic efficiency is

DOI: 10.1021/acscentsci.6b00389
ACS Cent. Sci. 2017, 3, 135–140

maintained at about 87%, 83%, and 81% at 0.5 mA cm^{-2} respectively after 50 cycles. When tested at a higher current density of 1.0 mA cm^{-2}, a Coulombic efficiency of 90% after 50 cycles is achieved for the modified electrode with 550@10 nm nanosphere coating. It is worth addressing that, for practical batteries, areal capacities >3 mAh cm^{-2} are needed. Cycling at various areal capacities (1.0, 2.0, and 4.0 mAh cm^{-2}) at a constant current density of 1.0 mA cm^{-2} has been performed as shown in Figure S5, which demonstrates improved Coulombic efficiency due to the coating of SiO_2@PMMA nanospheres. Additionaly, the Coulombic efficiency could be further improved by the use of lithium bis(trifluoromethanesulfonyl)-imide (LiTFSI, 1 M) in cosolvent of 1,3-dioxolane and 1,2-dimethoxyethane (DOL/DME, 1:1 by volume) with lithium nitrate (1 wt %)[26] as electrolyte or with electrolyte additives such as lithium polysulfide.[38]

Furthermore, AC impedance spectroscopy measurements of cells with Cu electrode with and without the nanosphere coating were taken to gain insight into the extent of dendrite growth during extensive cycling. Typical impedance spectra measured at various cycles of Li deposition/dissolution are given in Figures 4c and 4d. At high frequencies, the intercept with the *x*-axis corresponds to the ohmic resistance (R1 in the equivalent-circuit model) of the cell including the electrolyte resistance and contact resistances from electrode leads and terminals.[39] The semicircle at high and intermediate frequencies is ascribed to the electrode/electrolyte interface for the pristine cell, and the spike at low frequencies corresponds to lithium ion diffusion. It can be observed that the cell using the electrode coated with a layer of SiO_2@PMMA nanospheres has lower interfacial resistance (180 Ω) than the control electrode (230 Ω), due to the better wettability of the coating with the electrolyte (Figure S6). Meanwhile, the reduction of polarization (hysteresis) in the voltage profile during Li deposition/dissolution is shown in Figure S7, which confirms the lower polarization in the cell using the modified electrode. It is worth noting that, after the first cycle and 10th cycles of Li deposition/dissolution, the interfacial impedance gradually reduces. The drop in resistance is associated with the growth of lithium dendrites that increase the interfacial area between the electrolyte and lithium metal, which results in the reduction of resistance according to Li/electrolyte interface (R3).[39,40] Moreover, after 10 cycles, the semicircle is suppressed strongly and splits into two separate semicircles attributed to two different processes. The impedance spectroscopy of the cells after 10 cycles, together with well-fitted spectra, are shown in Figure 4d, demonstrating that the two separated semicircles are represented by two parallel combinations of resistance and capacitance from electrode/electrolyte interface in addition to the Li/electrolyte interface (Li dendrite). It indicates that, compared with the cell using bare Cu electrode (from 230 Ω to 42 Ω), the cell using core−shell nanophere coated electrode has less reduction of interfacial resistance (from 180 Ω to 45 Ω), implying the suppression of lithium dendrite growth.

Consequently, the coating of SiO_2@PMMA core−shell nanospheres plays a critical role in the uniform deposition of Li metal and the stability of SEI formation, an explanation for which should be considered here. The core−shell structure produces a synergistic effect between the core and shell to prevent Li dendrite growth. The SiO_2 core with high Young's modulus can suppress lithium dendrite growth. The nanoscaled pores formed by the coating of SiO_2@PMMA core−shell nanospheres are so small that lithium dendrites cannot penetrate the membrane, but Li ions can diffuse without being blocked. The PMMA shell is able to stick the SiO_2 spheres together to form a robust and flexible membrane that can accommodate volume change during Li deposition/dissolution without cracking and can also prevent reaction between SiO_2 and Li metal. In addition, Figure S6a,b shows the comparison of liquid electrolyte uptake between a commercial Celgard polyethylene separator and a SiO_2@PMMA membrane, which indicates a much larger electrolyte uptake for the latter. It is known that the dendrite growth is more pronounced when there is inhomogeneity of Li^+ flux. Hence the capability of absorbing electrolyte can make the lithium flux uniformly distributed across the Li metal surface. Moreover, commercial Celgard separator has a melting point of about 135 °C[41] and can lose dimensional stability upon exposure to high temperatures above 100 °C, as shown in Figure S6c. In sharp contrast, the freestanding SiO_2@PMMA membrane exhibits extremely small thermal shrinkage attributed to the inorganic SiO_2 core, indicating excellent thermal stability.

In summary, we have demonstrated a novel design of SiO_2@PMMA core−shell coating on lithium metal anode that can provide a cheap and facile approach to successfully suppress the growth of lithium dendrites. This SiO_2@PMMA coating also satisfies many other requirements, such as conduction of lithium ions, good mechanical and thermal stability, and high flexibility, owing to the synergistic effect of SiO_2 and PMMA. Improved cycling Coulombic efficiency was achieved for the electrode coated with SiO_2@PMMA nanospheres at various current densities and areal capacities. It is envisioned that the application of SiO_2@PMMA coatings for high-energy-density lithium metal batteries will contribute to improved safety and performance.

■ ASSOCIATED CONTENT

Supporting Information

The Supporting Information is available free of charge on the ACS Publications website at DOI: 10.1021/acscentsci.6b00389.

Complete experimental details and additional characterizations (PDF)

■ AUTHOR INFORMATION

Corresponding Author

*E-mail: yicui@stanford.edu.

ORCID

Wei Liu: 0000-0002-6206-8321

Notes

The authors declare no competing financial interest.

■ ACKNOWLEDGMENTS

Y.C. acknowledges the support from the Assistant Secretary for Energy Efficiency and Renewable Energy, Office of Vehicle Technologies of the U.S. Department of Energy under the Battery Materials Research (BMR) Program and the Battery 500 Consortium.

■ REFERENCES

(1) Armand, M.; Tarascon, J.-M. Building better batteries. *Nature* **2008**, *451*, 652−657.

(2) Bouchet, R.; Maria, S.; Meziane, R.; Aboulaich, A.; Lienafa, L.; Bonnet, J. P.; Phan, T. N. T.; Bertin, D.; Gigmes, D.; Devaux, D.; Denoyel, R.; Armand, M. Single-ion BAB triblock copolymers as

DOI: 10.1021/acscentsci.6b00389
ACS Cent. Sci. 2017, 3, 135−140

highly efficient electrolytes for lithium-metal batteries. *Nat. Mater.* **2013**, *12*, 452−457.
(3) Xu, W.; Wang, J.; Ding, F.; Chen, X.; Nasybulin, E.; Zhang, Y.; Zhang, J. G. Lithium metal anodes for rechargeable batteries. *Energy Environ. Sci.* **2014**, *7*, 513−537.
(4) Bruce, P. G.; Freunberger, S. A.; Hardwick, L. J.; Tarascon, J.-M. Li-O_2 and Li-S batteries with high energy storage. *Nat. Mater.* **2012**, *11*, 19−29.
(5) Yang, Y.; Zheng, G.; Cui, Y. Nanostructured sulfur cathodes. *Chem. Soc. Rev.* **2013**, *42*, 3018−3032.
(6) Ritchie, A.; Howard, W. Recent developments and likely advances in lithiumion batteries. *J. Power Sources* **2006**, *162*, 809−812.
(7) Flandrois, S.; Simon, B. Carbon materials for lithium-ion rechargeable batteries. *Carbon* **1999**, *37*, 165−180.
(8) Harry, K. J.; Hallinan, D. T.; Parkinson, D. Y.; MacDowell, A. A.; Balsara, N. P. Detection of subsurface structures underneath dendrites formed on cycled lithium metal electrodes. *Nat. Mater.* **2014**, *13*, 69−73.
(9) Bhattacharyya, R.; et al. In situ NMR observation of the formation of metallic lithium microstructures in lithium batteries. *Nat. Mater.* **2010**, *9*, 504−510.
(10) Jana, A.; Ely, D. R.; García, R. E. Dendrite-separator interactions in lithium-based batteries. *J. Power Sources* **2015**, *275*, 912−921.
(11) Aurbach, D.; Zinigrad, E.; Cohen, Y.; Teller, H. A short review of failure mechanisms of lithium metal and lithiated graphite anodes in liquid electrolyte solutions. *Solid State Ionics* **2002**, *148*, 405−416.
(12) Lu, Y.; Tu, Z.; Archer, L. A. Stable lithium electrodeposition in liquid and nanoporous solid electrolytes. *Nat. Mater.* **2014**, *13*, 961−969.
(13) Naoi, K.; Mori, M.; Naruoka, Y.; Lamanna, W. M.; Atanasoski, R. The surface film formed on a lithium metal electrode in a new imide electrolyte, lithium bis (perfluoroethylsulfonylimide)[LiN-$(C_2F_5SO_2)_2$]. *J. Electrochem. Soc.* **1999**, *146*, 462−469.
(14) Lee, Y. M.; Seo, J. E.; Lee, Y. G.; Lee, S. H.; Cho, K. Y.; Park, J. K. Effects of triacetoxyvinylsilane as SEI layer additive on electrochemical performance of lithium metal secondary battery. *Electrochem. Solid-State Lett.* **2007**, *10*, A216−A219.
(15) Crowther, O.; West, A. C. Effect of electrolyte composition on lithium dendrite growth. *J. Electrochem. Soc.* **2008**, *155* (11), A806−A811.
(16) Ding, F.; Xu, W.; Graff, G. L.; Zhang, J.; Sushko, M. L.; Chen, X.; Shao, Y.; Engelhard, M. H.; Nie, Z.; Xiao, J.; Liu, X.; Sushko, P. V.; Liu, J.; Zhang, J.-G. Dendrite-free lithium deposition via self-healing electrostatic shield mechanism. *J. Am. Chem. Soc.* **2013**, *135*, 4450−4456.
(17) Stark, J. K.; Ding, Y.; Kohl, P. A. Dendrite-free electrodeposition and reoxidation of lithium-sodium alloy for metal-anode battery. *J. Electrochem. Soc.* **2011**, *158*, A1100−A1105.
(18) Yoon, S.; Lee, J.; Kim, S.-O.; Sohn, H.-J. Enhanced cyclability and surface characteristics of lithium batteries by Li−Mg co-deposition and addition of HF acid in electrolyte. *Electrochim. Acta* **2008**, *53*, 2501−2506.
(19) Zhamu, A.; Chen, G.; Liu, C.; Neff, D.; Fang, Q.; Yu, Z.; Xiong, W.; Wang, Y.; Wang, X.; Jang, B. Z. Reviving rechargeable lithium metal batteries: enabling next-generation high-energy and high-power cells. *Energy Environ. Sci.* **2012**, *5*, 5701−5707.
(20) Matsuda, Y. Behavior of lithium/electrolyte interface in organic solutions. *J. Power Sources* **1993**, *43*−*44*, 1−7.
(21) Aurbach, D.; Zinigrad, E.; Cohen, Y.; Teller, H. A short review of failure mechanisms of lithium metal and lithiated graphite anodes in liquid electrolyte solutions. *Solid State Ionics* **2002**, *148*, 405−416.
(22) Yan, K.; Lu, Z.; Lee, H.-W.; Xiong, F.; Hsu, P.-C.; Li, Y.; Zhao, J.; Chu, S.; Cui, Y. Selective deposition and stable encapsulation of lithium through heterogeneous seeded growth. *Nature Eng.* **2016**, *1*, 16010.
(23) Lin, D.; Liu, Y.; Liang, Z.; Lee, H.-W.; Sun, J.; Wang, H.; Yan, K.; Xie, J.; Cui, Y. Layered reduced graphene oxide with nanoscale interlayer gaps as a stable host for lithium metal anodes. *Nat. Nanotechnol.* **2016**, *11*, 626−632.
(24) Liang, Z.; Lin, D.; Zhao, J.; Lu, Z.; Liu, Y.; Liu, C.; Lu, Y.; Wang, H.; Yan, K.; Tao, X.; Cui, Y. Composite lithium metal anode by melt infusion of lithium into a 3D conducting scaffold with lithiophilic coating. *Proc. Natl. Acad. Sci. U. S. A.* **2016**, *113*, 2862−2867.
(25) Liu, Y.; Lin, D.; Liang, Z.; Zhao, J.; Yan, K.; Cui, Y. Lithium-coated polymeric matrix as a minimum volume-change and dendrite-free lithium metal anode. *Nat. Commun.* **2016**, *7*, 10992.
(26) Zheng, G.; Lee, S. W.; Liang, Z.; Lee, H.-Y.; Yan, K.; Yao, H.; Wang, H.; Li, W.; Chu, S.; Cui, Y. Interconnected hollow carbon nanospheres for stable lithium metal anodes. *Nat. Nanotechnol.* **2014**, *9*, 618−623.
(27) Yan, K.; Lee, H.-W.; Gao, T.; Zheng, G.; Yao, H.; Wang, H.; Lu, Z.; Zhou, Y.; Liang, Z.; Liu, Z.; Chu, S.; Cui, Y. Ultrathin two-dimensional atomic crystals as stable interfacial layer for improvement of lithium metal anode. *Nano Lett.* **2014**, *14*, 6016−6022.
(28) Kim, J. S.; Kim, D. W.; Jung, H. T.; Choi, J. W. Controlled lithium dendrite growth by a synergistic effect of multilayered graphene coating and an electrolyte additive. *Chem. Mater.* **2015**, *27*, 2780−2787.
(29) Kamaya, N.; Homma, K.; Yamakawa, Y.; Hirayama, M.; Kanno, R.; Yonemura, M.; Kamiyama, T.; Kato, Y.; Hama, S.; Kawamoto, K.; Mitsui, A. A lithium superionic conductor. *Nat. Mater.* **2011**, *10*, 682−686.
(30) Seino, Y.; Ota, T. T. K.; Hayashi, A.; Tatsumisago, M. A sulphide lithium super ion conductor is superior to liquid ion conductors for use in rechargeable batteries. *Energy Environ. Sci.* **2014**, *7*, 627−631.
(31) Liu, Z.; Fu, W.; Payzant, E. A.; Yu, X.; Wu, Z.; Dudney, N. J.; Kiggans, J.; Hong, K.; Rondinone, J.; Liang, C. Anomalous high ionic conductivity of nanoporous β-Li_3PS_4. *J. Am. Chem. Soc.* **2013**, *135*, 975−978.
(32) Stone, G. M.; Mullin, S. A.; Teran, A. A.; Hallinan, D. T.; Minor, A. M.; Hexemer, A.; Balsara, N. P. Resolution of the modulus versus adhesion dilemma in solid polymer electrolytes for rechargeable lithium metal batteries. *J. Electrochem. Soc.* **2012**, *159*, A222−A227.
(33) Bogush, G. H.; Tracy, M. A.; Zukoski, C. F. Preparation of monodisperse silica particles: control of size and mass fraction. *J. Non-Cryst. Solids* **1988**, *104*, 95−106.
(34) Ge, J.; Hu, Y.; Zhang, T.; Yin, Y. Superparamagnetic composite colloids with anisotropic structures. *J. Am. Chem. Soc.* **2007**, *129*, 8974−8975.
(35) Mbese, J. Z.; Ajibade, P. A. Preparation and characterization of ZnS, CdS and HgS/Poly (methyl methacrylate) nanocomposites. *Polymers* **2014**, *6*, 2332−2344.
(36) Djian, D.; Alloin, F.; Martinet, S.; Lignier, H.; Sanchez, J.Y. Lithium-ion batteries with high charge rate capacity: influence of the porous separator. *J. Power Sources* **2007**, *172*, 416−42.
(37) Nestler, T.; Schmid, R.; Münchgesang, W.; Bazhenov, V.; Schilm, J.; Leisegang, T.; Meyer, D. C. Separators-technology review: ceramic based separators for secondary batteries. *AIP Conf. Proc.* **2013**, *1597*, 155−184.
(38) Li, W.; Yao, H.; Yan, K.; Zheng, G.; Liang, Z.; Chiang, Y. M.; Cui, Y. The synergetic effect of lithium polysulfide and lithium nitrate to prevent lithium dendrite growth. *Nat. Commun.* **2015**, *6*, 7436.
(39) Schweikert, N.; Hahn, H.; Indris, S. Cycling behaviour of Li/$Li_4Ti_5O_{12}$ cells studied by electrochemical impedance spectroscopy. *Phys. Chem. Chem. Phys.* **2011**, *13*, 6234−6240.
(40) Schweikert, N.; Hofmann, A.; Schulz, M.; Scheuermann, M.; Boles, S. T.; Hanemann, T.; Hahn, H.; Indris, S. Suppressed lithium dendrite growth in lithium batteries using ionic liquid electrolytes: Investigation by electrochemical impedance spectroscopy, scanning electron microscopy, and in situ ^{7}Li nuclear magnetic resonance spectroscopy. *J. Power Sources* **2013**, *228*, 237−243.
(41) Jeong, H. S.; Lee, S. Y. Closely packed SiO_2 nanoparticles/poly (vinylidene fluoride-hexafluoropropylene) layers-coated polyethylene separators for lithium-ion batteries. *J. Power Sources* **2011**, *196*, 6716−6722.

DOI: 10.1021/acscentsci.6b00389
ACS Cent. Sci. 2017, 3, 135−140